Available online at www.sciencedirect.com
SCIENCE DIRECT®
Physica B 358 (2005) 314–322
PHYSICA B
www.elsevier.com/locate/physb

# First-principles investigation of the alloying effect of refractory elements Ta and W in the misfit dislocation core of $\gamma/\gamma'$ (0 0 1) interface

C.Y. Geng[a,*], C.Y. Wang[a,b,c,d], T. Yu[a]

[a]*Institute of Functional Materials, Central Iron and Steel Research Institute, No. 76 Xueyuan Nanlu, Beijing 100081, China*
[b]*Department of Physics, Tsinghua University, Beijing 100084, China*
[c]*International Center for Materials Physics, Academica, Shenyang 110016, China*
[d]*CCAST (World Laboratory), P.O. Box 8730, Beijing 100080, China*

Received 9 November 2004; received in revised form 22 January 2005; accepted 22 January 2005

**Abstract**

By use of first-principles DMol method based on density functional theory, we investigated the alloying effect of refractory elements such as Ta and W in $a/2$ [1 1 0] (0 0 1) misfit dislocation core of the $\gamma/\gamma'$ interface in single-crystal Ni-base superalloys. The energetic calculations show that both the refractory elements can stabilize the $a/2$ [1 1 0] (0 0 1) misfit dislocation core. The analysis of the electronic structure indicates that there is charge accumulation between the refractory impurity atom and the neighboring Ni atoms, and the strong bonds between refractory impurities and Ni atoms are mainly due to the hybridization of impurity d-Ni d orbitals. The introduction of the two refractory impurities results in a strong pinning effect on the $a/2$ [1 1 0] (0 0 1) misfit dislocation motion in the $\gamma/\gamma'$ interface.


*PACS:* 71.15.Mb; 61.72.Lk; 68.35.−p; 61.66.Dk

*Keywords:* Misfit dislocation; Electronic structure; $\gamma/\gamma'$ interface; Refractory element; DMol; Superalloys

## 1. Introduction

Single-crystal Ni-base superalloys, used in gas turbine blade applications, are precipitation hardened by ordered $L1_2$ $Ni_3Al$ based intermetallic phase ($\gamma'$), which are coherent with the FCC matrix phase ($\gamma$). In addition to the size and distribution of the precipitates, the nature of the interface between the precipitates and the matrix plays an important role in determining the strength of the superalloys.

In recent years, increasing amounts of refractory elements (such as Re, Ta, W) were introduced in

*Corresponding author. Tel./fax: +086 010 621 82756.
*E-mail address:* gengcuiyu122@sohu.com (C.Y. Geng).

0921-4526/$ - see front matter © 2005 Elsevier B.V. All rights reserved.
doi:10.1016/j.physb.2005.01.467

Ni-base superalloys to improve the mechanical properties [1–4]. Re proved to be an especially effective solid solution strengthener and significantly enhanced the creep rupture life [1,5]. Ta is a more efficient hardener and has beneficial effect on single-crystal castability in reducing alloy freckle formation, plus it positively influences environmental properties [6,7]. W additions go into solid solution to provide solid solution strengthening [8]. As a result of the experimental efforts, it is now believed that Re, Ta, and W occupy Al sites in Ni-base superalloys [9,10]. Because of the importance of these refractory elements in designing new generation Ni-base superalloys, it is necessary to explore the relationship of their alloying effects with bonding between atoms. Some first-principles research studies [11–16] have been reported on this topic while systematic work on the $\gamma$–$\gamma'$ two-phase are relatively few [14–16]. Using the density functional for molecules (DMol) method [17,18], Chen et al. [14–16] investigated the individual strengthening effect and the synergetic effect of Re and Ru on the $\gamma/\gamma'$ interface. They use a completely coherent $\gamma/\gamma'$ interface cluster model to simulate the real interface approximately. While it is known from transmission electron microscopy (TEM) experiments [19–24] that due to the lattice mismatch between the two phases, misfit dislocations form readily with plastic deformation at high temperatures or with prolonged aging. From these studies it is now clear that the primary deformation mode at $\gamma/\gamma'$ interface is associated with $a/2$ $\langle 1\,1\,0\rangle$ Burgers vector misfit dislocations which are predominantly edge in character. As an important structural defect widely present in Ni-base superalloys, misfit dislocation has strong interactions with impurity, and the interaction greatly affect the mechanical properties of the superalloys. However, to our best knowledge, a fundamental understanding of the influence of the impurity on the $\gamma/\gamma'$ interface misfit dislocation based on first-principles method has not yet been established, although the electronic structure of refractory elements within the core region may play an important role in the impurity-misfit dislocation interactions. So in this paper, we performed the widely used first-principle DMol method to investigate the effect of refractory elements such as Ta and W in the $a/2$ [1 1 0] (0 0 1) misfit dislocation of $\gamma/\gamma'$ interface, in the hope of an accurate simulation of the $\gamma/\gamma'$ system will improve our understanding of the physical factors and the microscopic mechanisms that control the interfacial strength of Ni-base superalloys. The results for Re impurity are in preparation.

The paper is organized as follows. In Section 2, we briefly describe the cluster model and the first-principles DMol method used in our calculation. In Section 3, we present detailed results of the energetics and electronic structure of refractory elements such as Ta and W doped at misfit dislocation core. We summarize our results and conclusions in Section 4.

## 2. Method and computational model

In this work, we applied the first-principles DMol molecular cluster approach based on density functional theory (DFT) [25] to investigate the energetics and the electronic structure of refractory elements such as Ta and W doped in misfit dislocation core of $\gamma/\gamma'$ (0 0 1) interface. DMol used the localized numerical linear combination of atomic orbital (LCAO) as basis sets, has been widely applied to calculate various systems such as molecular clusters, chemisorption and surface reconstruction, etc. [13,17,26,27]. Using this method, some theoretical investigations have been successfully performed on the complex interactions between impurity and dislocations [28–30]. In our calculations, we have employed the double numerical polarized (DNP) basis and the local density approximation (LDA) correction [31] to obtain more precise results.

The cluster model of $a/2$ [1 1 0] (0 0 1) misfit dislocation of $\gamma/\gamma'$ interface in our calculations is constructed as follows. First, we reproduce the experimental situation [19–24]. Considering that the lattice parameters of Ni and $Ni_3Al$ are respectively $a(Ni) = 3.52\,\text{Å}$ and $a(Ni_3Al) = 3.568\,\text{Å}$, the $\gamma/\gamma'$ interface is then modeled by matching a $p(74 \times 74)$-Ni(0 0 1) slab (21 layers) with $p(73 \times 73)$-$Ni_3Al$(0 0 1) slab (21 layers) along the [0 0 1] direction ($z$-axis). Periodic boundary

conditions were employed in the $x$ and $y$ directions, and in the direction perpendicular to the interface, i.e. $z$ direction. The cells were terminated by free surfaces. Then, about 518,640 atoms are selected and relaxed by molecular dynamics (MD) method [32] using the Chen and Voter potentials [33,34]. The potentials employed for the atomistic simulations have been successfully used in studies of Ni, Al and $Ni_3Al$ grain boundaries [34–37] and surfaces [33,34,38]. The MD relaxation induces a pair of $a/2$ [1 1 0] (0 0 1) and $a/2$ [1 −1 0] (0 0 1) edge dislocations with equivalent dislocation core structures presented in the $\gamma/\gamma'$ interface, so we only study the $a/2$ [1 1 0] (0 0 1) misfit dislocation in a configuration with $C_{2v}$ symmetry.

We extract a cluster model of the $a/2$ [1 1 0] (0 0 1) dislocation core employed in our calculations, shown in Fig. 1. The model, which contains seven atomic layers with BABCBAB stacking sequence along [1 −1 0], has 175 atoms. The corresponding planes A, B and C in the middle five layers is presented in Figs. 1(a)–(c), respectively. In Fig. 1(d), the B and C planes (the two adjacent planes in the stacking sequence along [1 −1 0]) are marked by open and solid symbols. The size of the above cluster model was chosen to be large enough to guarantee that the essential features of electronic structure of Ni or Al in the dislocation core can be well described in the model without loss of significant accuracy. Due to their large radii and site preference, the refractory impurities Ta and W are placed in the position labeled 57, substituting for the corresponding Al atoms. Considering the effect of relaxation around these impurities, we perform structure optimizations by using DMol with the total energy minimization. During the optimizations, the outmost B layers are fixed, and only the neighboring Ni atoms around impurities in the middle five layers (all the atoms labeled by the numerals in Fig. 1) are allowed to relax. We used the optimized structures to investigate the effect of refractory elements Ta and W in the $a/2$ [1 1 0] (0 0 1) misfit dislocation of $\gamma/\gamma'$ interface. The convergence criteria for the energy gradient and the atomic displacement are 0.001 Ry/a.u. and 0.001 Å, respectively. The degree of convergence of the self-consistent iterations, measured by changes in the charge density, was set to 0.00001, which allowed the binding energy to converge to 0.00001 Ry.

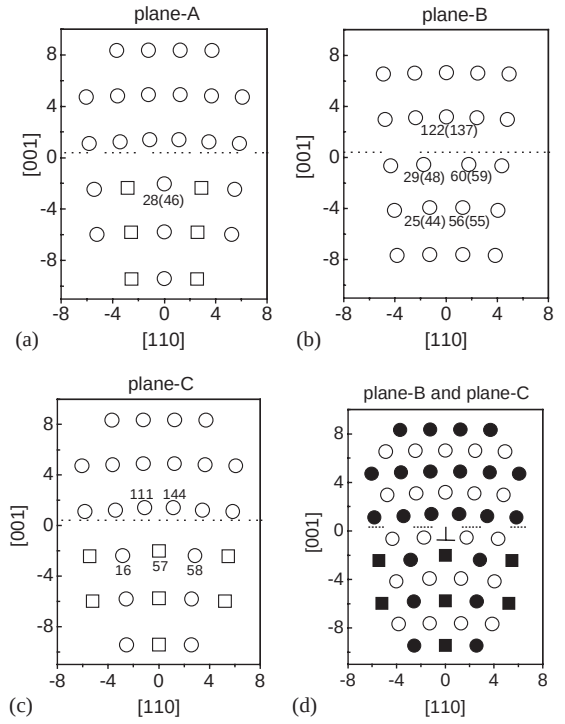


Fig. 1. Cluster model of the $a/2$ [1 1 0] (0 0 1) misfit dislocation core in the $\gamma/\gamma'$ interface. The dashed line represents the $\gamma/\gamma'$ interface, and the circle and square symbols denote Ni and Al atoms, respectively. Figs. 1(a)–(c) represent the corresponding planes A, B and C in the middle five layers. In Fig. 1(d), the B and C planes are marked by open and solid symbols, respectively.

## 3. Results and discussion

To avoid the possible insufficiency by the MD relaxation, we performed the DMol relaxation calculation on the initial pure misfit dislocation obtained by MD method and named the relaxed structure as the clean misfit dislocation. To examine the differences of the two structures, the clean misfit dislocation structure is shown as solid symbols and the initial pure misfit dislocation is shown as hollow symbols in Fig. 2. We find that there are only slight displacements in the middle layers plane B and C, and the difference of the

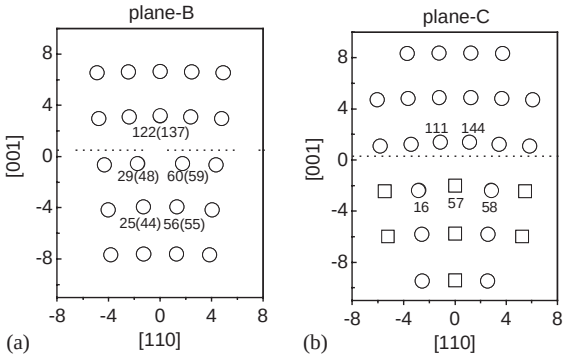


Fig. 2. Planes B and C of the cluster model used in the calculation. The atoms in the clean and the initial pure misfit dislocation core structure are shown as solid and hollow symbols, respectively. The dashed line represents the $\gamma/\gamma'$ interface, and the circle and square symbols denote Ni and Al atoms, respectively.

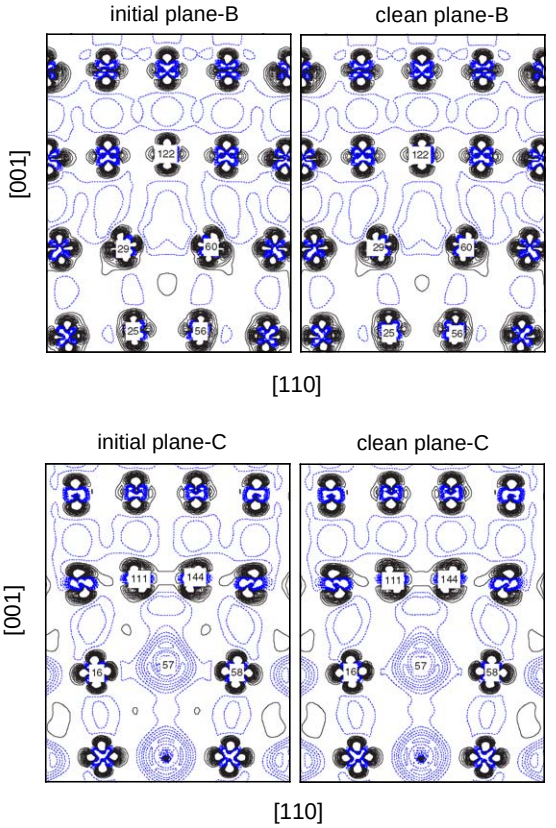


Fig. 3. Charge density difference of planes B and C before and after the DMol relaxation. The contour spacing is 0.01 ea.u.$^{-3}$. Solid lines and dashed lines correspond to the increased and the decreased charge density, respectively.

binding energies between the initial pure and the clean misfit dislocations is small, only 0.03 eV. It appears that for the study of the $a/2$ [1 1 0] (0 0 1) misfit dislocation of $\gamma/\gamma'$ interface, the initial pure misfit dislocation obtained by MD method is reliable. To see the influence of the relaxation on the electronic structure, charge density differences are shown in Fig. 3. Comparing the charge density distribution of the clean misfit dislocation with that of the initial one, we find though the initial misfit dislocation is a good approximation, the first-principles relaxation is essential.

In this section, we discuss the effect of refractory elements Ta, W in the $a/2$ [1 1 0] (0 0 1) misfit dislocation core of $\gamma/\gamma'$ interface. To understand the energetics effect induced by the refractory element atoms when placed at the Al 57site, we first define the impurity formation energy as

$$E_{\mathrm{imp}} = \frac{E_{\mathrm{b}}^{\mathrm{sub}} - E_{\mathrm{b}}^{\mathrm{clean}}}{N}, \qquad (1)$$

where $E_{\mathrm{b}}^{\mathrm{sub}}$ is the binding energy of the impurity substituted system, while $E_{\mathrm{b}}^{\mathrm{clean}}$ is the binding energy of the clean system. $N$ is the total number of the impurity atoms in the impurity-substituted system. As is known, the binding energy of a cluster is defined as $E_{\mathrm{b}} = E_{\mathrm{t}} - E_{\mathrm{a}}$, where $E_{\mathrm{t}}$ is the total energy of the cluster and $E_{\mathrm{a}}$ is the sum of free atomic total energies. The impurity formation energy of Ta and W in the $a/2$ [1 1 0] (0 0 1) misfit dislocation core of $\gamma/\gamma'$ interface is presented in Table 1. From the value of $E_{\mathrm{imp}}$, we find that both the two refractory impurities can stabilize the $a/2$ [1 1 0] (0 0 1) misfit dislocation core. Table 1 also lists the impurity formation energy of Ta and W in the perfect crystal (a 141-atom cluster without dislocation is shown in Fig. 4) for comparison. It can be seen that when substituted for the Al sites in the perfect crystal, the refractory impurities stabilize the structure too. From the change induced by the environment, it is clearly seen that Ta and W prefer to occupy the $a/2$ [1 1 0] (0 0 1) misfit dislocation core, that is, the $a/2$ [1 1 0] (0 0 1) misfit dislocation core of the $\gamma/\gamma'$ interface has a tendency to trap refractory impurity atoms. The

Table 1
The impurity formation energy $E_{imp}$ (eV) of Ta and W in the $a/2[1\,1\,0](0\,0\,1)$ misfit dislocation core of $\gamma/\gamma'$ interface and in the perfect crystal

| | Dislocation | Perfect crystal |
|---|---|---|
| Ta | −5.51 | −5.37 |
| W | −5.10 | −5.01 |

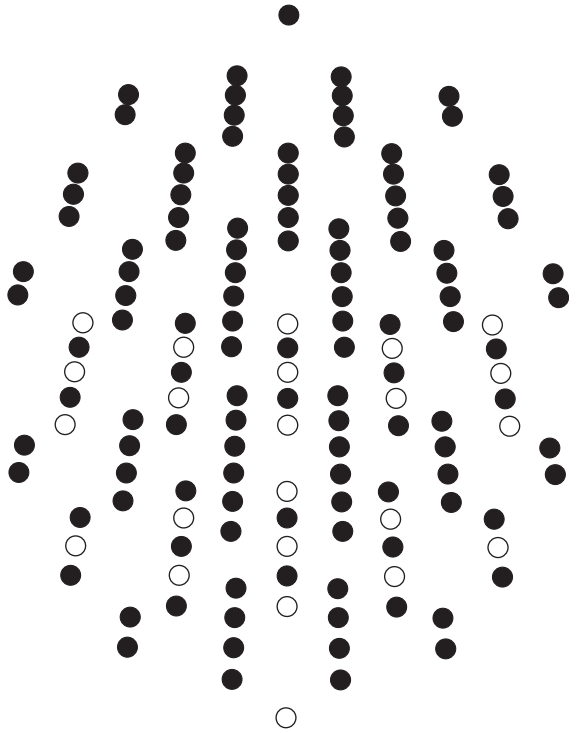

Fig. 4. Cluster model of the perfect crystal without dislocation in the $\gamma/\gamma'$ interface. The open and solid symbols denote Al and Ni atoms, respectively.

trapping effect of the dislocation core on refractory impurity atoms will potentially influence the dislocation mobility.

One can obtain directly an insight into the bonding character by charge density distribution. This can be best described by calculating the difference of charge density as follows:

$$\Delta\rho_{imp} = [\rho(dis_{sub}) - \rho_{free}(dis_{sub})] - [\rho(dis_{clean}) - \rho_{free}(dis_{clean})], \quad (2)$$

where $\rho(dis_{sub})$ and $\rho_{free}(dis_{sub})$ are the charge density of the bonding atom system and the free atom system for the refractory impurity substituted dislocation system $dis_{sub}$, while $\rho(dis_{clean})$ and $\rho_{free}(dis_{clean})$ are the charge density of the bonding atom system and the free atom system for the clean dislocation system $dis_{clean}$, respectively. We will refer to $\Delta\rho_{imp}$ as the impurity-induced charge density. The impurity-induced charge density on the planes C, B and $(1\,-1\,0)$, is shown in Figs. 5–7, respectively. Here solid and dotted curves represent contours of increased and decreased charge densities. From Fig. 5, we find that due to the refractory impurity atom substituted for the Al atom, the neighboring Ni atoms seem to lose electron compared with the clean dislocation systems. We can also see that, for both the refractory impurities-substituted systems, there is charge accumulation between the refractory impurity atom and the neighboring Ni atoms such as Ni16, Ni58, Ni111 and Ni144 in plane C. This means the bonding for refractory impurity atom and the neighboring Ni atoms in $dis_{sub}$ system is stronger than that for Al and the neighboring Ni atoms in $dis_{clean}$ system, and the introduction of refractory impurity atom can increase the interfacial cohesion strength of the interface. From Fig. 6, we can see that strong charge correlation regions due to the electron accumulation appear among atoms Ni25, Ni56, Ni29 and Ni60 in plane

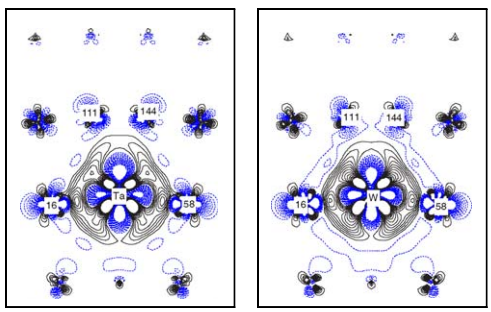


(a) (b)

Fig. 5. The impurity-induced charge density on plane C. Figs. 5(a) and (b) represent Ta and W induced charge density, respectively. The contour spacing is 0.002 ea.u.$^{-3}$. Solid lines and dashed lines correspond to the increased and the decreased charge density, respectively.

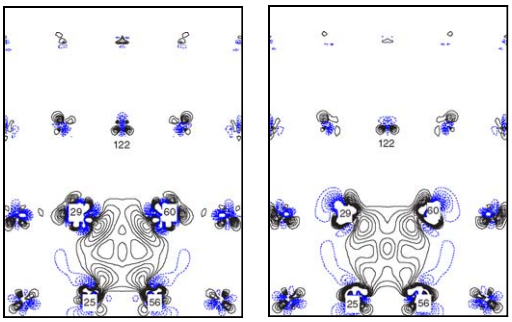


(a) (b)

Fig. 6. The impurity-induced charge density on plane B. Figs. 6(a) and (b) represent Ta and W induced charge density, respectively. The contour spacing is 0.002 ea.u.$^{-3}$. Solid lines and dashed lines correspond to the increased and the decreased charge density, respectively.

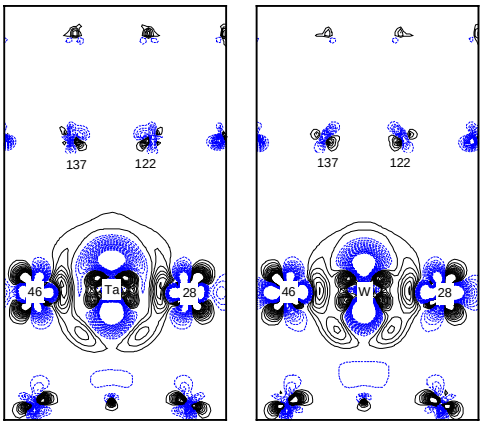


(a) (b)

Fig. 7. The impurity-induced charge density on the (1 −1 0) plane. Figs. 7(a) and (b) represent Ta and W induced charge density, respectively. The contour spacing is 0.002 ea.u.$^{-3}$. Solid lines and dashed lines correspond to the increased and the decreased charge density, respectively.

B. Thus, relatively strong bonds are formed among Ni atoms (such as Ni25, Ni56, Ni29 and Ni60) and the cohesive strength is increased too. Furthermore, From Figs. 7(a) and (b), we can easily find that the interplanar bonding between the refractory atom of plane C and Ni atoms (such as Ni28 and Ni46) of plane A are also enhanced. The above charge density analysis reflect the strong pinning effect of refractory impurities on the $a/2$ [1 1 0] (0 0 1) misfit dislocation core of $\gamma/\gamma'$ interface, which should affect the microscopic mechanical properties of single-crystal Ni-base superalloys.

In order to analyze the interactions between the impurities and host atoms further, we calculated the density of states (DOS). Considering the local symmetry around atom 57, we only give the nonequivalent Ni atoms of the neighboring Ni atoms. Energies are given relative to the Fermi level. Two main atomic bonding features can be observed in Fig. 8. First, compared with Al states, the main peaks of refractory impurities locate at a relative lower energy region, so the d DOS of the neighboring Ni atoms such as Ni28, Ni29 and Ni25 are moved slightly towards the lower energy part as a result of impurity d-Ni d hybridization. In addition, for the Ni atoms (Ni28, Ni29 and Ni25) in the $dis_{sub}$ systems, there are some changes in the d DOS at the corresponding location of the refractory impurities' main peaks, which indicate the enhanced interactions between the d orbitals of the refractory atoms and those of the Ni atoms. Thus, the strong bonds between impurity and Ni atoms are formed mainly due to the hybridization of impurity d-Ni d. From the DOS analysis, we see that refractory impurities strongly hybridizes with host Ni atoms in the $a/2$ [1 1 0] (0 0 1) misfit dislocation core of $\gamma/\gamma'$ interface.

It is well known that the charge transfer between the alloying element and the host atom play an important role in the formation of interatomic bonding. Table 2 lists the Mulliken population in every valence orbital of refractory impurity and its neighboring Ni atoms. From Table 2, it can be seen that for the $dis_{clean}$ system there are charge transfer from Ni-4s to Ni-3d orbitals, and from the Al-3s to the Al-3p orbitals, thus resulting in the Ni d–d bonding and hybridization between Ni-d and Al-p orbitals. It also can be seen that charge transfers occur from Al atoms to Ni atoms, which is the representative characteristic for $Ni_3Al$ system. In the $dis_{sub}$ systems, Ta and W impurities both obtains charge from the neighboring Ni atoms and assigns them mainly to 5d valence orbitals. This is consistent with charge density

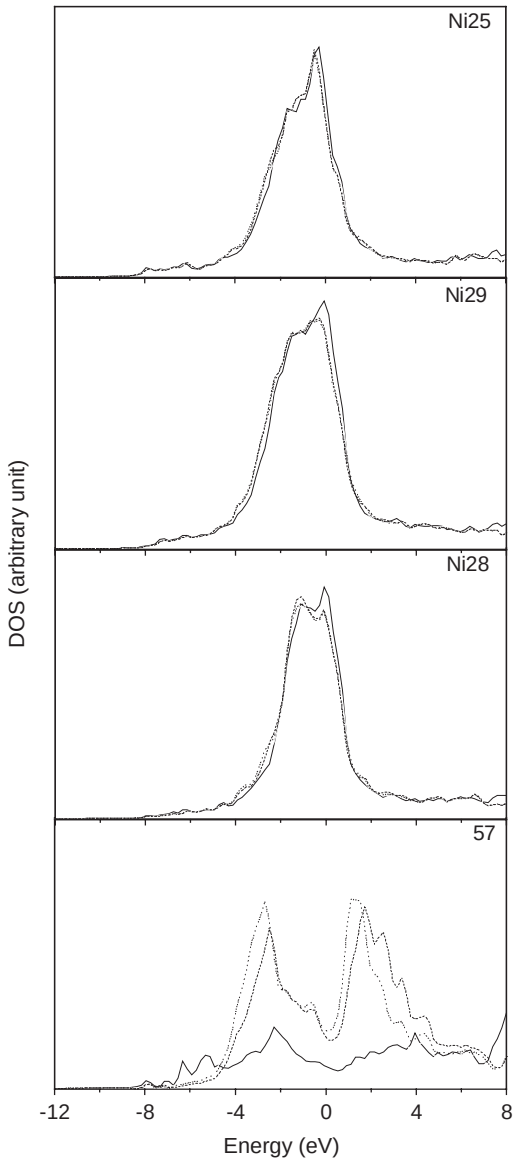


Fig. 8. DOS for refractory impurities and the neighboring Ni atoms in the $a/2$ [1 1 0] (0 0 1) misfit dislocation core of $\gamma/\gamma'$ interface. The thick solid lines denote DOSs of the clean dislocation system, dashed lines and dotted lines denote DOSs of Ta and W substituted dislocation system, respectively. The Fermi level is shifted to zero. The Arabic numbers in 57, Ni28, etc., correspond to those in Fig. 1.

analysis in Figs. 5–7. Compared with the $\mathrm{dis}_{\mathrm{clean}}$ system, the Ni atoms gain relatively fewer charges and transfer more 4s and 4p charge to 3d orbitals

Table 2
Mulliken populations $N_{\mathrm{clean}}$ ($N_{\mathrm{sub}}$) in every valence orbital of refractory impurity and its neighboring Ni atoms in the $\mathrm{dis}_{\mathrm{clean}}$ ($\mathrm{dis}_{\mathrm{sub}}$) system

| | | $N_{\mathrm{clean}}$ | $N_{\mathrm{sub}}^{\mathrm{Ta}}$ | $N_{\mathrm{sub}}^{\mathrm{W}}$ | $\Delta Q^{\mathrm{Ta}}$ | $\Delta Q^{\mathrm{W}}$ |
|---|---|---|---|---|---|---|
| Atom57 | 3(6)s | 1.075 | 0.419 | 0.413 | | |
| | 3(6)p | 1.325 | 0.677 | 0.706 | | |
| | 3(5)d | 0.366 | 4.046 | 5.126 | | |
| | $Q$ | −0.234 | 0.137 | 0.243 | 0.371 | 0.477 |
| Ni28 | 4s | 0.759 | 0.759 | 0.754 | | |
| | 4p | 0.454 | 0.441 | 0.448 | | |
| | 3d | 8.840 | 8.822 | 8.809 | | |
| | $Q$ | 0.057 | 0.027 | 0.016 | −0.03 | −0.041 |
| Ni29 | 4s | 0.724 | 0.729 | 0.720 | | |
| | 4p | 0.497 | 0.496 | 0.496 | | |
| | 3d | 8.831 | 8.811 | 8.799 | | |
| | $Q$ | 0.057 | 0.041 | 0.021 | −0.016 | −0.036 |
| Ni25 | 4s | 0.725 | 0.726 | 0.722 | | |
| | 4p | 0.505 | 0.501 | 0.504 | | |
| | 3d | 8.842 | 8.829 | 8.820 | | |
| | $Q$ | 0.078 | 0.063 | 0.053 | −0.015 | −0.025 |
| Ni16 | 4s | 0.676 | 0.664 | 0.660 | | |
| | 4p | 0.530 | 0.525 | 0.526 | | |
| | 3d | 8.836 | 8.826 | 8.824 | | |
| | $Q$ | 0.048 | 0.021 | 0.015 | −0.027 | −0.033 |
| Ni111 | 4s | 0.679 | 0.673 | 0.669 | | |
| | 4p | 0.521 | 0.522 | 0.523 | | |
| | 3d | 8.796 | 8.794 | 8.795 | | |
| | $Q$ | 0.000 | −0.006 | −0.008 | −0.006 | −0.008 |
| Ni122 | 4s | 0.687 | 0.687 | 0.687 | | |
| | 4p | 0.568 | 0.568 | 0.569 | | |
| | 3d | 8.784 | 8.784 | 8.784 | | |
| | $Q$ | 0.044 | 0.044 | 0.045 | 0.000 | 0.001 |

$\Delta Q^{\mathrm{Ta}} = Q_{\mathrm{sub}}^{\mathrm{Ta}} - Q_{\mathrm{clean}}$, etc., where $Q_{\mathrm{clean}}$ ($Q_{\mathrm{sub}}$) is the net number of electrons in the valence orbital for refractory impurity and its neighboring Ni atoms in the $\mathrm{dis}_{\mathrm{clean}}$ ($\mathrm{dis}_{\mathrm{sub}}$) system. Here $Q = N - Z_{\mathrm{val}}$, where $Z_{\mathrm{val}}$ is the standard number of valence electrons per atom.

to balance the lose of charge due to the presence of refractory impurities, thus to strengthen the hybridization between impurity d and Ni-d states. The above results are consistent with the analysis on charge density and DOS.

In general, the behavior of refractory impurities (such as Ta and W) and their influence on the host atoms have similarities. The interfacial cohesion strength of the interface was enhanced by the

hybridization between impurity d and Ni-d orbitals, resulting in a strong pinning effect on the $a/2$ [1 1 0] (0 0 1) misfit dislocation motion in the $\gamma/\gamma'$ interface. These results provide a basis for understanding the physical factors and the microscopic mechanisms that control the interfacial strength of single-crystal Ni-base superalloys.

## 4. Conclusions

We have studied the alloying effect of refractory elements such as Ta and W in $a/2$ [1 1 0] (0 0 1) misfit dislocation core of $\gamma/\gamma'$ interface using first-principles DMol method. The calculated impurity formation energy shows that the introduction of refractory impurities significantly stabilizes the $a/2$ [1 1 0] (0 0 1) misfit dislocation core. In addition, the charge distribution and DOS results indicates that some charge accumulation regions appear between the refractory impurity atoms and the neighboring Ni atoms, and the strong bonds between them mainly due to the hybridization of impurity d-Ni d orbitals. In summary, the refractory impurities induces a strong pinning effect on the $a/2$ [1 1 0] (0 0 1) misfit dislocation motion in the $\gamma/\gamma'$ interface, which is related with the mechanical properties of the single-crystal Ni-base superalloys.

## Acknowledgments

We are grateful to Dr. S.Y. Wang, Dr. J. Wu and Prof. F.H. Wang for beneficial discussions. This work is supported by "973 Project" from the Ministry of Science and Technology of China (Grant no. TG2000067102) and the National Natural Science Foundation of China (Grant no. 90306016, 901041044).

## References

[1] A.F. Giamei, D.L. Anton, Metall. Trans. 16 A (1985) 1997.
[2] K. Harris, G.L. Erickson, S.L. Sikkenga, W. Brentnall, J.M. Aurrecoechea, K.G. Kubarych, in: S.D. Antolovitch, et al. (Eds.), Superalloys, Warrendale, 1992, p. 297.
[3] A.D. Cetel, D.N. Duhl, in: D.N. Duhl, et al. (Eds.), Superalloys, Warrendale, TMS, 1988, p. 235.
[4] M.V. Nathal, L.J. Ebert, Metall. Trans. A 16 (1985) 1863.
[5] D. Blavette, P. Caron, T. Khan, Scripta Metall. 20 (1986) 1395.
[6] M. Gell, D.N. Duhl, A.F.Giamei, Proceedings of 4th International Symposium on Superalloys, Seven Springs, 1980, p. 205.
[7] K. Harris, G.L. Erickson, R.E. Schwer, Directionally solidified and single crystal superalloys, in: J.R. Davis, et al. (Eds.), Metals Handbook, vol. 1, tenth ed., ASM Int, America, 1991, p. 995.
[8] M.J. Donachie, S.J. Donachie, in: M.J. Donachie, S.J. Donachie (Eds.), Superalloy, ASM Int, America, 2002, p. 103.
[9] H. Murakami, Y. Saito, H. Harada, in: R.D. Kissinger, D.J. Deye, D.L. Anton, et al. (Eds.), Superalloys, TMS, Warrendale, 1996, p. 249.
[10] H. Murakami, H. Harada, H.K.D.H. Bhadeshia, Appl. Surf. Sci. 76/77 (1994) 177.
[11] J.H. Xu, T. Oguchi, A.J. Freeman, Phys. Rev. B 36 (1987) 4186.
[12] A.V. Ruban, H.L. Skriver, Phys. Rev. B 55 (1997) 856.
[13] S.Y. Wang, C.Y. Wang, J.H. Sun, W.H. Duan, D.L. Zhao, Phys. Rev. B 65 (2001) 035101.
[14] K. Chen, L.R. Zhao, J.S. Tse, Philos. Mag. 83 (2003) 1685.
[15] K. Chen, L.R. Zhao, J.S. Tse, Mater. Sci. Eng. A 360 (2003) 197.
[16] K. Chen, L.R. Zhao, J.S. Tse, Acta Mater. 51 (2003) 1079.
[17] B. Delley, J. Chem. Phys. 92 (1990) 508.
[18] B. Delley, J. Chem. Phys. 94 (1991) 7245.
[19] A. Lasalmonie, J.L. Strudel, Philos. Mag. 32 (1975) 937.
[20] M. Feller-Kniepmeier, T. Link, Mater. Sci. Eng. A 113 (1989) 191.
[21] C. Carry, J.L. Strudel, Acta Metall. 26 (1978) 859.
[22] A.K. Singh, N. Louat, K. Sadananda, Metall. Trans. A 19 (1988) 2965.
[23] G.C. Weatherly, R.B. Nicholson, Philos. Mag. 17 (1968) 801.
[24] D.F. Lahrman, R.D. Field, R. Darolia, H.L. Fraser, Acta Metall. 36 (1988) 1309.
[25] P. Hohenberg, W. Kohn, Phys. Rev. B 136 (1964) 864; W. Kohn, L.J. Sham, Phys. Rev. A 140 (1965) 1133.
[26] L. Ye, A.J. Freeman, B. Delley, Phys. Rev. B 39 (1989) 10144.
[27] S.P. Tang, A.J. Freeman, B. Delley, Phys. Rev. B 45 (1992) 1776.
[28] Y. Niu, S.Y. Wang, D.L. Zhao, C.Y. Wang, Comp. Mater. Sci. 22 (2001) 144.
[29] Y. Niu, S.Y. Wang, D.L. Zhao, C.Y. Wang, J. Phys.: Condens. Matter 13 (2001) 4267.
[30] J.A. Yan, C.Y. Wang, W.H. Duan, S.Y. Wang, Phys. Rev. B 69 (2004) 214110.
[31] J.P. Perdew, Y. Wang, Phys. Rev. B 45 (1992) 13244.
[32] M.P. Allen, D.J. Tildesley, Computer Simulation of Liquids, Oxford University Press, New York, 1987, p. 83.

[33] A.F. Voter, S.P. Chen, Proc. Mater. Res. Soc. Symp. 82 (1987) 175.
[34] S.P. Chen, D.J. Srolovitz, A.F. Voter, J. Mater. Res. 4 (1989) 62.
[35] S.P. Chen, A.F. Voter, D.J. Srolovitz, Scripta Metall. 20 (1986) 1389.
[36] S.P. Chen, A.F. Voter, D.J. Srolovitz, Proc. Mater. Res. Soc. Symp. 81 (1987) 45.
[37] S.P. Chen, A.F. Voter, R.C. Albers, A.M. Boring, P.J. Hay, J. Mater. Res. 5 (1990) 955.
[38] S.P. Chen, A.F. Voter, D.J. Srolovitz, Phys. Rev. Lett. 57 (1986) 1308.